TITLE:

Conditions of submarine levéed channel inception: Examination by flume experiments

Running Title:

Conditions of submarine levéed channel inception

AUTHORS:

Justine Poppeschi[1]*, Kazushi Nakata[2] and Hajime Naruse[1]

Address:

1. Graduate School of Science, Kyoto University, Kitashirakawa Oiwakecho, Sakyo-ku, Kyoto, 606-8502 Japan
2. Kobe University, 1-1, Rokkodai-cho, Nada-ku, Kobe, 657-8501, Japan

* Corresponding author email: justine.poppeschi@gmail.com

Associate Editor – Anna Pontén

ABSTRACT

Submarine levéed channels are often observed in submarine fans, although submarine fans without continuous levéed channels are also common depending on the composition of supplied sediments, particularly the proportion of muddy/sandy materials. However, parameters governing the inception of levéed channels have not yet been studied. Furthermore, depositional levéed channel topography has not been simulated in experimental flumes in any previous study conducted with dilute flows (flow concentration <10%). Herein, four experimental series were conducted (Series A, B, C and D) to simulate depositional submarine channels and to study their formative conditions. A mixture of sediment and saline water was used in the experiments, and both the width of an outlet diffuser and flow discharge rate were varied in the experimental series. A topography composed of a channel with two ridges resembling natural depositional submarine channels with levées was formed in all experiments. Comparisons between the experimental topographies and natural submarine fans revealed that the two of four experimental series produced channel levées with length to width ratios similar to those produced by natural systems. An experiment with half the outlet size produced a channel two time deeper (4.5 cm against 2.0 cm and 2.2 cm) as compared to other experiments. The flow discharge rate and outlet width were half of those observed in Series A and B. Furthermore, salt was removed from the initial mixture for one of the experiments, resulting in high natural levées with a short channel. This study demonstrated that dilute flows could form purely depositional channel levées without precursor or resultant erosive features. In addition, results revealed that the formation of submarine channels is related to two factors: channel width and muddy suspended sediment.

Keywords: Channel levée inception; deep-sea morphology; depositional processes; flume experiment; submarine fans; turbidity currents

(A) INTRODUCTION

Aggradational levées border submarine channels in muddy fan settings, which are usually composed of successive layers formed by overspilling, and are cumulative stack records of system formations. The development and architecture of levées is governed by parameters such as flow velocity and channel height, as well as the diameter, grain size and concentration of suspended particles (Skene *et al.*, 2002; Pirmez & Imran, 2003). Straub and Mohrig (2008) investigated the effect of these parameters in flume experiments based on the assessment of flow conditions and the sedimentary properties of the modern event in the Bruneian offshore system. They showed that the flow confinement and sediment concentration profiles in channel–levée morphology are factors governing levée growth. Further, studies have found that the stability of these morphologies depends on other hydraulic conditions (Komar, 1971; Pirmez & Imran, 2003; Janocko *et al.*, 2013). The topographic features of channel–levée complexes and conditions suitable for their inception and development have been detailed in previous studies (Straub & Mohrig, 2008; Spinewine *et al.*, 2011; Dorrell *et al.*, 2015; Leeuw *et al.*, 2016); however, none of these have succeeded in simulating depositional submarine channel–levée systems with dilute flows (low concentration turbidity currents; sediment concentration of <10%).

It is difficult to assess the conditions suitable for channel inception and the role of muddy materials in controlling the diversity in channel morphology because it is impossible to directly observe this process in nature. The inception of new channel–levée systems takes years as turbiditic events occur irregularly and it is difficult to predict their locations. Thus, it is necessary to conduct flume experiments in laboratories under controlled flow conditions with *in situ* measurements to understand these processes satisfactorily. Several studies have been conducted to simulate channel–levée morphology and to study their governing parameters (Garcia, 1990; Métivier *et al.*, 2005; Wormleaton *et al.*, 2005; Keevil *et al.*, 2006; Yu *et al.*, 2006; Leeuw *et al.*, 2016). Métivier *et al.* (2005) demonstrated that a dense bottom current could produce lobes followed by a channel incision, depending on parameters such as slope, initial discharge, sediment flow composition and concentration, and the Shields nondimensional bed shear stress; the latter was used to calculate the initiation of the sediment movement in channels. Further, an aggradational mound feature was initially formed, and then a channel incised the mound. A saline flow was used in this experiment to simulate fine materials in natural systems. Because there was no suspended sediment in the dense flow used, the aggrading natural levée was not reproduced in the experiments of Métivier *et al.* (2005).

コメントの追加 **[S1]:** ? the experiments of Métivier *et al.* (2005)

Some studies have successfully reconstructed the suitable conditions required for levéed channel inception, exclusively with pre-existing erosional features. For example, Fildani *et al.* (2012) combined flume experiments, analysis of existing natural systems and two datasets with numerical analysis, and proposed that channels are formed during the erosional phase at the inception; similar to that demonstrated by Métivier *et al.* (2005). Those authors hypothesized that aggrading levées could only form after the erosion phase and channel formation. This hypothesis was supported by other studies (Maier *et al.*, 2013; Covault *et al.*, 2014). In these studies, cyclic steps, scours or alternative gaps were considered important for channel inception and maintenance because they provide initial confinement for turbidity currents and allow the levées to aggrade. Rowland *et al.* (2010) studied depositional levéed channels without the use of erosional features to confine the flow and explained that levéed channel development was impossible without partial confinement. Rowland *et al.* (2010) assumed that the levées were formed by the coarse fraction of the suspended load. In addition, that study utilized a nonerodible bed to avoid confinement by erosion. However, the produced morphologies in the study did not achieve self-confinement. Therefore, Rowland *et al.* (2010) concluded that an incision is an essential prerequisite for channel–levée development. Conversely, Leeuw *et al.* (2016) suggested that the depositional aspects need to be considered and indicated that confinement at the inception and development of levées occurs because of the sediment deposition. Further, those authors emphasized that transitionally rough conditions are essential for producing levéed channel systems because entrainment is necessary to produce channel features.

Despite numerous experiments regarding levéed submarine channels, the effect of fine-grained mud in the sediment gravity flow on the development of levéed channels has not been fully investigated, since reproducing the entrainment process of muddy materials at an experimental scale is difficult. Many studies have highlighted the importance of muddy suspensions in the formation of channel–levée systems wherein sand-sized grains produce topographic features, while mud-sized grains provide excess density to drive flows (Sequeiros *et al.*, 2010; Spinewine *et al.*, 2011). However, most previous studies on the inception of channel–levée systems, including that of Leeuw *et al.* (2016), employed sand-sized sediments. Even when clay particles were used, the cohesive nature of the particles inhibited the natural behaviour of turbidity current sedimentary processes at small scales. In their review, Wells and Dorrell (2021) demonstrated that increasing stratification in turbidity current layers reduced the magnitude of turbulent shear stress and that saline water created conditions closer to natural flows. Therefore, the present study replaced clay particles with salt in the initial mixture to generate the turbidity currents and promote levée formation without the perturbation due to the cohesive nature of the clay particles.

Therefore, this study used saltwater as a mud analogue to densify the experimental turbidity currents. Although salt is not deposited as mud particles, the behaviour of a fluid that

コメントの追加 **[S2]:** ? the present

has gained excess density by containing mud can be reproduced with saltwater (Sequeiros *et al.*, 2010). Since muddy sediments take considerable time to settle, their prolonged suspension maintains a sustained driving force (i.e. excess density) in the flow. Fine-grained sediments have long been implicated in the development of aggrading levéed channel systems (Deptuck and Sylvester, 2017), and the approach taken herein aims to reproduce the behaviour of muddy sediments. Most flume experiments on levéed channel inception in submarine fans have not utilised salt for increased flow density (Rowland *et al.*, 2010; Fildani *et al.*, 2012). However, several studies have found that using salt results in a dense bottom current that reproduces the flow structures in a channel–levée morphology (Keevil *et al.*, 2006; Peakall *et al.*, 2007; Straub & Mohrig, 2008). Thus, the constant mixing ratio of particles was used for the mixture in the fourth experimental series; however, salt was omitted to quantify its impact (density) on channel–levée morphologies.

Another factor possibly governing submarine channel inception is the geometry of the flow at the downstream end of the submarine canyon. Although the width of the submarine canyons (hundreds of metres to several kilometres) is much larger than the flow thickness (<100 m), in experimental studies, the inlet size is usually much narrower than the produced flow thickness (e.g. Imran *et al.*, 2002). The horizontal velocity field may be different between shallow and deep flows spreading radially from a point source; however, the effect of this flow geometry on the formation of submarine levées has not been examined satisfactorily in previous studies. Thus, herein, the developmental conditions for levéed channels were examined at two different settings of flow geometry at the inlet.

Four experimental series were performed to produce purely aggradational channel–levée systems that developed from a nonerodible bed without any confinement. The experiments used a mixture of either saline or fresh water and sediments composed of plastic and small amounts of siliciclastic particles. The channel–levée morphologies obtained herein were produced in each experiment by depositional processes only with normalized dimensions similar to those of natural systems, such as the Amazon channel (Jegou *et al.*, 2008) and the Delgada channel (Normark & Gutmacher, 1983). Each morphology was produced under hydraulic conditions of flow that have not been assessed previously (Leeuw *et al.*, 2016). This study provides an improved understanding of the parameters that govern the inception of levéed channel.

(A) METHODS

(B) Experimental setup

The experimental flume tank was located at Kyoto University (Fig. 1). The dimensions of the tank basin were 4.8 m in length, 2.2 m in width and 1.5 m in depth. The water level inside the tank was kept constant. A plastic board was placed at the bottom of the tank to represent a nonerodible bed with a slope of 10%. A higher slope percentage than natural conditions is used in these flume experiments to increase the bed shear stress of the flow. Two mixing tanks (0.45 m^3) were used to stir plastic particles, salt and water using a propeller and pump installed at the bottom of each tank. To prevent return flow of the turbidity current during the experiments, a drainage output was installed at the end of the flume tank to empty the water. The flow discharge was measured using an electromagnetic flow meter (LR 5061; HIOKI, Japan). The volumetric discharge rate for Experimental Series A, B, C and D was set at 3.0, 3.0, 1.5 and 3.0 L/s, respectively. Five types of plastic and siliciclastic particles were used during the experiments. Their granulometry (in millimetres) and density (ρ in $g \cdot cm^{-3}$) are presented in Table 1 and Fig. 2. Coloured siliciclastic sands were used to better visualize the sedimentary features on the media and measurement tools. The quantity of sintering pigments used to dye siliciclastic sand was not enough to change the density of the sand grains. For each run of Series A, the initial particle concentrations in the mixing tanks were set at 18%.

The concentrations for runs 1, 2 and 3 of Series B were 21.5%, 22.6% and 19.7% (v/v), respectively. The initial concentrations for Series C were 20.1%, 20.3% and 20.1% (v/v). For Series D, the concentrations were 21.2%, 18.3% and 19.7% (v/v). The density of the saltwater used to produce the turbidity current was 1131 kg·m^{-3}.

(B) Examined flow boundary conditions

Herein, two experimental settings were assessed to study the factors affecting the formation of submarine channels: the inlet width and the presence of saltwater. Four series of experiments, namely A, B, C and D comprising three runs each, were conducted. The pump continuously injected sediments and the saltwater mixture into the flume tank through a diffuser with holes (diameter of 1 cm) placed 1 cm apart. A long diffuser (44 cm) was used in Series A, B and D. However, a short diffuser (22 cm) was used to simulate a point source case in Series C. For the point source case, the flow velocity is supposed to decrease rapidly because of the radial expansion of the flow geometry, while it is assumed to be maintained for a distance in the case of long diffusers (Fig. 2). Saltwater was used in Series A, B and C, while freshwater was used in Series D to confirm the effect of muddy water on channel formation.

(B) Measurements

An acoustic Doppler current profiler (ADCP; Vectrino Profiler; Nortek Inc., Rud, Norway) was used to measure the vertical profile of the flow velocity. The profiler is a high-resolution acoustic velocimeter that uses the three-dimensional Doppler effect to measure velocity fluctuations. The velocity meter was moved laterally from the start position to measure the velocity field during the experiments; the measurements were averaged every 30 s and the measurement locations are plotted in Fig. 3. The flow height was measured by recording a video of the flow and taking the value on a ruler placed on the side of the tank. The concentration of salt and sediment particles of turbidity currents was measured by direct sampling using an array of syphons of 10 tubes placed 1 cm apart. For each experimental run, syphon locations were changed to observe the flow composition and concentration at different points.

After three runs for each experimental series (A, B, C and D), the topography was manually measured using a scale. Measurements were performed on horizontal grids with a spacing of 5 or 10 cm. The analysed areas covered 3.0, 5.94, 4.86 and 3.24 m² in Series A, B, C and D, respectively. Following the measurement, a digital elevation model was constructed using ArcGIS (version 10.6.1). To compare the size of the four topographies produced with modern channel–levée systems, cross-sectional horizontal and vertical coordinates *x* and *z* were normalized by the width of each channel *W* (where *W* is defined as the distance between two maximum heights for the levées).

Samples acquired by the syphon and those collected from the bed were analysed using a settling tube grain size analyser (Naruse, 2005) and were subsequently processed using STube software (version 1.0).

(B) Calculations of the hydraulic parameters

The hydraulic conditions of the experimental flows were assessed as follows. Shear velocity u^* was calculated from the velocity profile measured by ADCP, assuming that the lower part of the density flow followed a logarithmic profile (Clauser, 1956) over the inner region of the lower shear layer (Appendix 1, Dorrell *et al.*, 2019). Then, the particle Reynolds number ($\mathrm{Re_p}^*$) was calculated as follows (Leeuw *et al.*, 2016; defined by Van Rijn, 1993):

$$\mathrm{Re_p}^* = \frac{u^* d}{\nu},$$

where u^*, d and ν denote the shear velocity ($\mathrm{m \cdot s^{-1}}$), mean diameter (m) of the particles and the kinematic viscosity ($\mathrm{m^2 \cdot s^{-1}}$) of the flow, respectively. The Shields parameter τ^* is the dimensionless bottom shear stress defined as follows:

$$\tau^* = \frac{u^*}{Rgd},$$

where $R = \frac{\rho_{\mathrm{sed}} - \rho_{\mathrm{salt}}}{\rho_{\mathrm{salt}}}$, ρ_{sed} is the density of sediments (the siliciclastic sediment density has been neglected as very small amount was used and only for the visualization of the topography), ρ_{salt} is the density of saltwater, g is the acceleration due to gravity ($\mathrm{m \cdot s^{-2}}$) and d is the mean diameter (m) of the particles.

The layered averaged velocity u is estimated from u^* as follows:

$$u = \frac{u*}{\sqrt{C_{\mathrm{f}}}},$$

where C_{f} is the friction coefficient (dimensionless). The densimetric Froude number, Frd, is expressed as follows:

$$\mathrm{Frd} = \frac{u}{\sqrt{\frac{\Delta\rho}{\rho}Cgh}} = \frac{u}{\sqrt{\frac{\rho_t - \rho_{fw}}{\rho_{fw}}Cgh}},$$

where $\rho_t = (\rho_{\mathrm{sed}} - \rho_{\mathrm{salt}}) \times C + \rho_{\mathrm{salt}} \times (1 - C)$, ρ_{fw} represents the density ($\mathrm{kg \cdot L^{-1}}$) of fresh water inside the main tank, C denotes the concentration (% v/v) of the sediments in the flow; the mixture was composed of 96% plastic particles and 4% red, green and yellow siliciclastic particles added to aid the visualization of sedimentary features. The parameter u denotes the mean velocity ($\mathrm{m \cdot s^{-1}}$) of the flow, and h is the height (m) of the flow. The parameters used in the calculations are presented in Table 2.

(A) RESULTS

(B) Hydrodynamics

The four series of experiments, A, B, C and D, produced density flows in subcritical conditions (Table 3). Figure 4 shows a visual representation of the flow evolving during the three runs. The flow was spread laterally towards the downstream end of the tank (Fig. 4A) in the first run of every experimental series. In the second run, the flow was partially confined between ridges created during the first run (Fig. 4B), and in the third run, the flow was mainly confined between the ridges.

The flow conditions measured at the centre of the experimental domain were largely different in velocity and concentration from those measured on the sides (Fig. 5; Appendices 1–3). The concentration and velocity values used here are all depth-averaged values. The velocity and concentration decreased from 0.348 to 0.006 $m \cdot s^{-1}$ and from 0.51% to 0.13% (v/v), respectively, from the centre to the side of the tank. The flow velocity profiles taken at different locations during each run (Fig. 3) are plotted in Figs 5 and A1 for the Series B, C and D (values for Series A were not measured).

(B) Channel–levée topographies

Channel topography with linear levées was observed after the experimental runs of all four series (Figs 6 and 7). Measurements of the produced topographies were recorded at the end of each experiment. The channel developed from the diffuser inlet to the centre of the experimental domain, and two levées developed on the flanks of the channel. The channel terminated with a rounded edge, and a lobate depositional feature developed at the end of the channel downstream. The channel floor was completely covered by a thin sedimentary layer; thus, the plastic board was not exposed. The channel had a length of 100 to 200 cm and a width of 20 to 100 cm (Fig. 7). Topographic relief between the channel floor and the lateral levées ranged from 0.1 to 5.1 cm in the upstream region, whereas the height of the levées decreased downstream. Series A and B (Fig. 7) were proportionally similar, unlike Series C, where the dimensions of the central channels were halved in length and width, but the height of the levées was doubled. The difference between the four series was distinct on the transect perpendicular to the flow direction at 75 cm from the diffuser (Fig. 8). Even though the channels formed in Series A, B and D were wider than those formed in Series C, the levées developed in the latter were twice as high as those developed in the former series. However, the plan view of the shape remained significantly similar in each case. The channel topography formed in Series D was much shorter than those of the other series (only 120 cm in length), but the levées were as high as in Series A and B. The shapes of the central channel topography differed slightly from the others.

(B) Grain-size distribution

For granulometry, sediment samples were collected from the middle of the channel for every experiment. Further, as the flow was assumed to build a symmetrical morphology around the central axis, only the right ridge was sampled. Granulometry results from upstream to downstream are presented in Fig. 9. The mean grain size of the deposits at the upstream and downstream ends of the channel ranged from 0.177 to 0.257 mm and 0.275 to 0.344 mm, respectively. For the levées, the mean grain size of the deposit at the upstream and downstream ends ranged from 0.188 to 0.238 mm and 0.206 to 0.238 mm, respectively. The grain size increased along with the increase in the distance from the source for both the levées and the channels in all experiments. In Series A and B, where a long channel was formed, there was a small difference in grain size between the channel and the natural embankment; whereas, in Series C and D, where only a short, circular depression was formed, there was a substantial difference in grain size between the two regions.

(B) Bedforms

Along with the channel–levée topography, bedforms were observed as shown in Fig. 10. They were located outside the channel with their crests extended obliquely in the levée's direction, and located in the regions between the levée crests and the lateral ends of the produced topography. Conversely, bedform crests developed transversely in the elongation direction of the channels on the lobate topography located downstream. The dimensions and granulometry for Series B and C are presented in Table 4, and they ranged from 6.0 to 9.75 cm in wavelength and 0.3 to 0.7 cm in height. It was found that the wavelengths of the bedforms were high in the downstream regions. Further, bedform shapes were asymmetrical, with the stoss side being longer than the lee side. However, the bedform migration direction was not observed during the experiments and hence the type of bedform produced could not be ascertained.

(A) DISCUSSION

(B) Comparison with natural systems

The topographies produced during the four experimental series were possibly analogous to channel–levée morphologies. The results in Series A and B were proportionally similar to natural systems. Following the normalization presented in the *Methods* section, cross-sections of the topography produced during the flume experiments were compared with those of the natural levéed channels observed in modern submarine fans (Figs 10 and 11). The *W*/*H* ratio (width to depth of the channel) and *L*/*H* ratio (length to depth of the channel) were also used to compare the dimensions of the morphologies obtained (Table 5, Fig. 11). The results of the four series were plotted against four channels in modern fans: the Amazon channel (Jegou *et al.*, 2008); Villafranca channel in the deep waters off the coast of Sicily (Hansen *et al.*, 2015); main channel on the Delgada fan in Northern California (Normark &

Gutmacher, 1983) and the channel from the Congo submarine fan, located at the mouth of the Zaire River (Savoye *et al.*, 2009), as shown in Fig. 12.

The chosen systems represent a variety of channel–levée systems created under different conditions (including sediment supply, discharge, concentration and seabed condition). The Amazon channel is a single channel–levée complex with an abundant supply of fine sediments (Pirmez & Irman, 2003). The Delgada channel is a good analogue because of its characteristics; it is not uniform, with the size of the levées and the width of the channel decreasing longitudinally, and its shape on the southern and northern lobes varies unexpectedly because of the low amount of supplied sediment (Normark & Gutmacher, 1983). The Villafranca channel has high rates of overspilling because of the high amount of sediment input from the nearby volcanic arc, providing a high aggradation rate for building levées (Gamberri *et al.*, 2011). The Congo channel is one of the channel systems with the thinnest sediment supply in the world, with a low ratio of sand/mud but high silt and clay amounts (Babonneau *et al.*, 2010).

The results of the experimental series were also compared with other natural systems (offshore Brunei, Straub & Morhig (2008); Lucia Chica channel, central California, Maier *et al.* (2013); Yellow and Blue Channels, Morhig and Buttles (2007); Amazon channel, Jegou *et al.* (2008); Delgada fan, Normark & Gutmacher (1983) and Congo channel (Savoye *et al.*, 2009)). Series A and B were found to be similar in proportion for the W/H ratio. The cross-sections of the ridges resembled natural levées of modern submarine channels, and the floor of the channel-like topography was slightly higher than the ambient basin plain of the natural system. Furthermore, Series A and B were proportionally similar to modern systems in width and height, such as the Lucia Chica channel (Maier *et al.*, 2013). Series C was disproportional to the other series. The W/H ratio observed in this series was significantly lower than the ratios of natural systems (Table 5). Its proportions are closer to a canyon system with high walls than a channel–levée system (for example, the *W*/*H* ratio of the offshore Brunei canyon system is 13.2).

The *L*/*H* ratio for the four experimental series is significantly lower than that of the natural systems (range 41.4–105.3 for flume experiments compared to 406.8–23000 for natural systems). The main reason why the *L*/*H* ratio differs so much is the limited length of the experimental tank. The channel system length cannot reach the same distance as natural systems that develop at several hundreds of kilometres. The comparison of the *L*/*H* ratio seems less relevant than the *W*/*H* ratio, because of the scale difference, which does not affect the width of the channel of the experiments.

(B) Comparison with existing flume experiments

Herein, Series A and B generated channel–levée systems with a much larger *L*/*H* ratio than other studies using a nonerodible bed. Although Rowland *et al.* (2010) produced a similar morphology as a channel system, the *L*/*H* ratio of the channel in that study was 72.7 to 75 for their Series F and H (Table 5). The present study is similar to the study by Rowland *et al.* (2010) in terms of the usage of a nonerodible bed. However, the length of the inlet to release the sediment used in our Series A, B and D was 40 cm long, compared to the study of Rowland *et al.* (2010), which used a 20 cm inlet. The use of salt in the initial mixture for the case of this study added density and helped to build the levées. Also, the slope used (10%) is steeper than the one used in the experiments of Rowland *et al.* (<1%), which helped to carry sediment for a longer distance, as it increased the flow velocity. This leads to entirely different topographies in the shape and length obtained (produced ridges in round shape, lateral deposits spreading too broadly, more than twice the size of the diffuser) for the majority of the experiments conducted.

コメントの追加 **[S3]:** ? The present

Herein, the use of a sufficiently broad line source instead of a point source is presumed to have played a significant role in the formation of long natural levées. For a point source as flow inlet, the flow spreads out radially and the velocity decelerates downstream at the same rate, forming a circular natural levée. Hence, the formation of a long channel is difficult. Whereas, when a broad line source is used, there is a zone in the centre of the source where no deceleration occurs; thus, a relatively long channel can be formed, and the natural levées are deposited along this channel. As the actual turbidity flow is expected to be much shallower than the channel width, the experimental setup of this study is more realistic than that of the previous studies.

The fact that the particle size did not change in the downstream direction in the Series A and B means that the flow was approximately constrained by the levées and continued to maintain a uniform flow condition. Thus, the flows in these experimental series achieved the self-confinement conditions; this is not the case for the study conducted by Rowland *et al.* (2012), where flow conditions were insufficient to suspend the sediments. The study by Leeuw *et al.* (2016) used an erodible bed, and they obtained confinement of the flow using the depositional process first and then erosional channelization. In Series A and B of this study, there was no difference in grain size between the channels and levée regions, whereas the natural levée deposits are much finer-grained than the channel deposits. This may be due to the use of saltwater as an analogue for mud, which is not deposited like natural systems.

(B) Significance of grain-size distribution in the formation of submarine levéed channel systems

Without examining the various formative conditions, depositional levéed channel morphology was quite easily simulated in this study, which could also be attributed to the various grain-size distributions and the use of saline water. Earlier studies, including that of Rowland *et al.* (2010), noted that aggraded levéed channel systems were difficult to reproduce. Thus, special conditions were needed to simulate them in the experimental scales. In contrast, because channel–levée systems are ubiquitous (Mutti & Normark, 1987) and can be induced under broader conditions than those previously estimated, these conditions can be used to model channel–levée morphology for natural systems. In natural conditions, channel–levée systems on submarine fans develop differently based on the material supplied (Reading & Richard, 1994).

Several studies have indicated that the grain-size segregation between the channel and levée is critical for the formation of levéed channel systems (Posamentier & Kolla, 2003; Spinewine *et al.*, 2011). Consequently, the sediment composition is different in channels and levées (Normark, 1970; Clark & Pickering, 1992). In levéed channel systems, the flow is confined and sandy materials are deposited on the channel floor and levées. Thus, turbidity currents can maintain their density because of fine materials (i.e. mud). However, it is difficult to model muddy suspensions at an experimental scale because the dimensionless index parameters for sediment transport, such as the Shields τ^* for silt (30 μm), are significantly higher in natural turbidity currents (200 for the flow velocity and the friction coefficient of 5.0 $m \cdot s^{-1}$ and 0.0004, respectively). If clay particles are used in the flume experiments, τ^* for the silt suspension decreases to <2 when the flow velocity is <0.5 $m \cdot s^{-1}$. Thus, in the study by Rowland *et al.* (2010), the impact of suspended particles was not adequately considered even though the flow shear stress exceeded the suspension threshold. However, the present study successfully accounted the effect of suspended particles using saltwater in the initial mixture to replace the finest mud sediments, which is essential for imparting density to the flow. Although the flow conditions in natural systems were unknown and those in this study may have been quite different from natural systems, the depositional levéed channel systems were successfully modelled in this study by adding a densifying material (i.e. saline water).

Experimental settings using a mixture of plastic particles and saline water enabled the formation of a purely aggradational system that was developed from a flat topography. Previous studies have indicated that the relief created by repeated turbidity currents is presumably erosional during the initial state and that aggraded channels develop after the levées are built due to overspilling (Fildani *et al.*, 2012; Maier *et al.*, 2013). However, the channel–levée morphologies obtained in the four experimental series were produced purely by deposition, which contradicts the hypothesis made in the previous studies. Series D was conducted without using salt in the experimental mixture. Consequently, the density of the turbidity currents was less contrasted with the ambient water density, which allowed for a more significant overspilling than in previous experiments. Thus, the flow could not be maintained for the same distance as in Series A and B. This result corroborates the hypothesis of Ezz *et al.* (2013), who showed that increasing the percentage of salt in the initial mixture yields a more confined flow without causing stripping or overspilling. There was no more deposition at the bottom of the channel, and the flow carried the sediment over a long distance.

After establishing the conditions for turbulent and critical flows, the Shields parameter and Reynolds number (Table 3) were used to compare the flows obtained in different studies using a Shields diagram (Fig. 13) (Alexander *et al.*, 2001; Yu *et al.*, 2006; Rowland *et al.*, 2010; Xu, 2010; Eggenhuisen & McCaffrey, 2011; Leuuw *et al.*, 2016). Although the suspension initiation is inherent to the particle concentration, especially in high concentration flow (Dorrell *et al.*, 2018), a low concentration flow is used herein [0.263%–0.96% (v/v)]; hence, the concentration is unaccounted for in the calculations of the Shields parameter and the Reynolds number (Table 3). The conditions for Series A and B herein were above that for the initiation of motion (as defined by Shields, 1936) and above that for the initiation of suspension (as defined by Niño *et al.,* 2003). The results implied that the flow could entrain and suspend particles.

It should be noted that the flow basal boundary condition was between the hydraulically smooth and transitionally rough conditions in the experiments conducted herein (Fig. 13). Leeuw *et al.* (2016) suggested that the flow conditions for developing channel–levée morphology should be transitionally rough boundary conditions (Garcia, 2008). However, the flow conditions for almost all experimental runs in Series A and B were at the limit between hydraulically smooth and transitionally rough boundary conditions. Thus, the results of this study proved that the transitionally rough boundary conditions were not a prerequisite for levéed channel formation. This may be related to the fact that this study used salt as an analogue for mud particles. Even in the hydraulically smooth conditions, very fine-grained material can remain suspended for extended periods. Therefore, if the grain-size distribution of the sediments is sufficiently wide, simple hydraulically smooth/rough conditions may not necessarily govern the conditions for the formation of levéed channels.

(B) Flow geometry and the formation of levéed channels

The flow inlet appears to have a stimulating effect on the development of the channel–levée systems. In Series C of this study, levées were twice as high and the channels were half as long as those in the other series. This significantly deviated from the proportions of natural systems and was clearly due to the half outlet size. The reduced outlet size confined the flow around the outlet and produced higher levées than those produced in the other experimental series. Further, as the flow discharge was halved, the flow velocity was insufficient to transport sediments at the same distance. This explains the shorter length of the channel for Series C as compared to the other three.

The relation between the inlet width and the conditions for forming a levéed channel can be explained as follows: if the inlet width is narrower than the flow thickness, the flow radially expands to the entire region (Fig. 14). Consequently, the velocity of the turbidity current is isotropically decelerated. Then, an arc-like deposition occurs at a certain distance from the inlet because of the flow deceleration. The resulting landform is a circular erosion feature (channel) and a very short and high natural levée. However, if the inlet width is broader than the flow thickness, the lateral expansion of the flow occurs only at inlet edges (Fig. 14). Thus, the flow velocity remains approximately constant in the area from the centre of the inlet downstream. In other words, sedimentation occurs from both ends of the inlet in the downstream direction due to the deceleration associated with the flow expansion; however, the centre of the flow can remain in an erosive or no-sediment state. Consequently, long natural levées are formed extending downstream from both ends of the inlet, while an almost bypassing flow forms a channel between the levées.

The lateral velocity variation in Series B supports the above hypothesis (Fig. 5). The degree of velocity deceleration in the channel and at the natural levée differs. From the channel centre to the top of the natural levée, the velocity does not decrease significantly in the lateral direction (Fig. 5). However, the flow is significantly decelerated on the side where the natural levée is deposited. This suggests that the flow geometry governed by the inlet width is related to the levéed channel. In fact, the lateral velocity variation in Series B supports the above hypothesis (Fig. 5). In actual submarine fans, the relationship between the width of a submarine canyon and the discharge of turbidity currents may significantly affect the stability of the levéed channel.

(B) Dissimilarities in topographic features with the natural submarine channel–levée systems

This study does not aim to reconstruct the hydrograph of turbidite currents in a submarine channel; thus, some architectural elements of the submarine channel–levée system are disregarded by this simplification. Terraces along the channel were not formed in the experiments; however, they are frequently described structures in the external and internal regions of natural levées (Hansen *et al.*, 2015). Also, while upstream-migrating sediment waves are typical topographic features of the submarine levées (Normark *et al.*, 1980), bedforms built outside the levées were not investigated herein due to the lack of migration direction data.

Although saltwater is not an exact analogue of muddy water, the experiments performed herein exhibited the significance of excess density imparted by fine-grained materials in creating a channel–levée system. Eliminating the negative effect of using clay minerals on the similarity law of the experiment, this study attempted to clarify a part of the formation mechanism of the channel–levée system by experimenting with a simplified setting. Nevertheless, the absence of clay in the initial mixture can consequently impact levée formations. In modern channel–levée systems, levée deposits are mainly composed of silt and clay (e.g. Zaire's levées, Gervais *et al.*, 2001; Cascadia's levées, Griggs & Kulm, 1970; Monterey's levées, Komar, 1969). The levées produced in the experimental series herein comprised coarse particles (levées' granulometry values 0.194–0.331 mm), which are closer to sand particles than clay particles (levées' granulometry values 2.0–0.2 μm). The turbidity currents are vertically differentiated in grain size inside, and the accumulation of fine-grained material from the upper part of the flow causes the natural levées to be highly aggraded. Thus, the addition of smaller particles with cohesive behaviour could produce more stable and prominent levées than those produced in this experimental study (Cantelli *et al.*, 2011).

The simplification of the experimental setup may cause a difference in the results of this study and the actual seafloor. For example, the grain size of the channel–levée system does not agree with the previous records. Natural levées are usually comprised of finer materials, such as clay or silt, as reported by Gervais *et al.* (2001). The grain size in channels is coarser than that in the levées in the natural systems, contrary to that observed in the fourth experimental series. Moreover, the size of the levée usually decreases from the supply source of the sediment (Hiscott *et al.*, 1997), which is not the case for the fourth experimental series. As shown in Fig. 7, the levée height in the experiments tends to increase from the supply source towards the end of the depression. This trend is in contrast with the majority of modern and ancient channel–levée systems. The absence of clay in the initial mixture of this study is evidently the reason for the difference in the grain size for the levées produced in this study and for those in the modern and ancient channel–levée systems. The experimental flows herein accumulated coarse grained deposits at the end of the channel downstream, whereas thick mounds did not necessarily form in the natural channel-lobe transition zone (Kane *et al.*, 2017). The topography obtained by this study may be similar to that of plunge pools (Lee, 2002). However, plunge pools are mainly erosional features, which are different from the depositional features observed herein.

In addition, the channel length to width ratios (L/W ratio) did not accurately match those of the modern channel–levée systems (Table 5). In the experimental series, the L/W ratio was between 1.8 and 4.0, which is far from the ratio for modern channel–levée systems, such as the incredibly long Amazon channel with L/W ratio 300.6. This difference in geometry may be due to the lack of fine-grained material in the experimental materials. Further, the size of the flume tank could be a reason for the low length achieved by the channel. Also, the time duration of the experiments was relatively short (*ca* 15 min). In other words, the experiment only captured the early stages of a channel–levée system before its growth.

There are limitations in the experimental techniques applied herein that can be improved in future studies, and therefore, the results have several characteristics that differ from those in natural systems. Nonetheless, this study adds to the understanding that submarine channels can develop without any erosional features under dilute flow conditions and presents a novel approach for forming channel–levée systems with turbidity currents using a mixture of plastic particles and salt. Further, it suggests that the relative width of inlets may contribute to the formation of a stable channel–levée system. It remains to be confirmed in future studies whether these results are qualitatively and quantitatively consistent with natural system processes.

(A) CONCLUSIONS

Herein, submarine channel–levée morphologies were obtained as purely depositional features through flume experiments. Four experimental series with three runs each were performed, and two of them exhibited significant correlations with modern fan systems. The channel–levées morphologies obtained for Series A and B experiments were found to be similar to the morphology of the Lucia Chica channel (Maier *et al.*, 2013). In contrast, the morphology obtained for Series C experiments was proportionally closer to the canyon morphology. This was attributed to the small dimensions of the experimental flow inlet in Series C.

The obtained morphology was produced under unexpected flow conditions for hydraulically smooth boundary conditions. Considering that channel–levée systems are quite common (Mutti and Normark, 1987), their inception and development can now be considered to involve several conditions. In addition, the conditions reported prior to this study did not consider the role of fine sediments in turbidity currents. Herein, the substitution of fine materials with saltwater facilitated the formation of channel–levée systems, reducing the flow overspill and aggrading the levées.

This study improved current understanding of the parameters governing the levéed channel inception, although uncertainty persists because the channel depth and the grain-size distribution for natural systems differ from those observed herein. Additionally, the number of experimental runs should be increased to achieve conditions similar to turbidity currents to improve our understanding of such parameters in natural systems. Further, an erodible bed could be employed for future studies, presumably resulting in the formation of channel–levée systems with different boundary conditions and consequently affecting the shape of the system.

ACKNOWLEDGEMENTS

We thank the reviewers for their comments and suggestions that greatly improved the quality of the paper. Also, we would like to thank the Dynamics Research Consortium (funded by JX, JOGMEC, INPEX and JAPEX), for funding this research.

DATA AVAILABILITY STATEMENT

The data that support the findings of this study are openly available in 4TU. Centre for Research Data at reference number uuid:6895547b-b3cd-45cf-ae07-4628a2dc10b4.

REFERENCES

Alexander J. (2008) Bedforms in Froude-Supercritical Flow, In: *Marine and river dunes dynamics conference volume*, pp. 1–5, Leeds University, U.K..

Cantelli A., Pirmez C., Johnson S. and Parker G. (2011) Morphodynamics and stratigraphic evolution of self-channelized subaqueous fans emplaced by turbidity currents. *Journal of Sedimentary Research*, **81**, 233–247.

Clark J.D., Kenyon N.H. and Pickering K.T. (1992) Quantitative analysis of the geometry of submarine channels: implications for the classification of submarine fans. *Geology*, **20**, 633-636.

Clauser F.H., (1956), The turbulent boundary layer, In: *Advances in Applied Mechanics* (H.L. Dryden and von Karman, eds.), 4, pp. 1–51.

Covault J.A., Kostic S., Paull C.K., Ryan H.F. and Fildani A. (2014) Submarine channel initiation, filling and maintenance from sea-floor geomorphology and morphodynamic modelling of cyclic steps. *Sedimentology*, **61**, 1031 –1054.

Destuck M.E. and Sylvester Z., (2017) Submarine fans and their channels, levees and lobes. *Submarine Geomorphology*, Springer Geology, 273-299

Dorrell, R. M., Peakall, J., Sumner, E. J., Parsons, D. R., Darby, S. E., Wynn, R. B., Özsoy, E. and Tezcan, D. (2016) Flow dynamics and mixing processes in hydraulic jump arrays: Implications for channel-lobe transition zones. *Marine Geology*, **381**, 181-193.

Dorrell, R. M., Amy, L. A., Peakall, J., & McCaffrey, W. D. (2018) Particle size distribution controls the threshold between net sediment erosion and deposition in suspended load dominated flows. *Geophysical Research Letters*, **45**, 1443-1452.

Dorrell, R. M., Peakall, J., Darby, S. E., Parsons, D. R., Johnson, J. and Sumner, E. (2019) Self-sharpening induces jet-like structure in seafloor gravity currents. *Nature communications*, **10**, 1–10.

Eggenhuisen J.T. and McCaffrey W.D., (2012), The vertical turbulence structure of experimental turbidity currents encountering basal obstructions: implications of vertical suspended sediments distribution in non-equilibrium currents. *Sedimentology* **59**, 1101–20.

Fildani A., Hubbard S.M., Covault J.A., Maier K.L., Romans B.W., Traer M. and Rowland J.C. (2012) Erosion at Inception of Deep-Sea Channels. *Marine and Petroleum Geology*, **41**, 48-61.

Hansen L.A.S., Callow R.H.T., Kane I.A., Gamberi F., Rovere M., Cronin B.T. and Kneller B.C. (2015) Genesis and Character of Thin-Bedded Turbidites Associated with Submarine Channels. *Marine and Petroleum Geology*, **67**, 852–79.

Garcia M.H. (1990) *Depositing and eroding sediment-driven flows: turbidity currents*. PhD Thesis, University of Minnesota, St. Anthony Falls Hydraulic Laboratory.

Garcia M. (2008) *Sedimentation Engineering: Processes, Measurements, Modelling and Practise.* American Society of Civil Engineers, Reston, VA, 1132 pp.

Gervais A., Mulder T., Savoye B., Migeon S. and Cremer M. (2001) Recent processes of levee formation on the Zaire deep-sea fan. *Comptes Rendus de l'Academie des Sciences-Series IIA-Earth and Planetary Science*, **332**, 371–378.

Griggs G.B. and Kulm L.D. (1970) Sedimentation in Cascadia Deep-Sea Channel. *GSA Bulletin*, **80**, 1361–1384.

Hansen L.A.S, Callow R.H.T., Kane I.A., Gamberi F., Rovere M., Cronin B.T. and Kneller B. (2015) Genesis and character of thin-bedded turbidites associated with submarine channels. *Marine and Petroleum Geology*, **67**, 852–879.

Hiscott R.N., Hall F.R. and Pirmez C. (1997) Turbidity-current overspill form the Amazon channel: texture of the silt/sand load, paleoflow from anisotropy of magnetic susceptibility and implications for flow processes, *Proceedings of the Ocean Drilling Program, Scientific Results,* **155**, 53–78.

Imran, J., Parker, G. and Harff P. (2002) Experiments on incipient channelization of submarine fans. *Journal of Hydraulic Research*, **40**, 21–32.

Janocko M., Nemec W., Henriksen S. and Warchoł M., (2013) The Diversity of Deep-Water Sinuous Channel Belts and Slope Valley-Fill Complexes. *Marine and Petroleum Geology,* **41**, 7–34.

Jegou I., Savoye B., Pirmez C. and Droz L. (2008) Channel-mouth lobe complex of the recent Amazon Fan: The missing piece. *Marine Geology,* **252**, 62–77.

Kane I.A., Kneller B.C., Dykstra M., Kassem A. and McCaffrey W.C. (2007) Anatomy of a submarine channel-levee: An example from Upper Cretaceous slope sediments, Rosario Formation, Baja California, Mexico. *Marine and Petroleum Geology*, **24**, 540–563.

Kane I.A., Ponten A.S.M., Vangdal B., Eggenhuisen J.T., Hodgson D.M. and Spychala Y.T. (2017) The stratigraphic record and processes of turbidity current transformation across deep-marine lobes. *Sedimentology*, **64**, 1236–1273.

Keevil G.M., Peakall J., Best J.L. and Amos K.J. (2006) Flow structure in sinuous submarine channels: Velocity and turbulence of an experimental submarine channel. *Marine Geology*, **229**, 241 –257.

Kneller B.C. and McCaffrey W.D. (2003) The interpretation of vertical sequences in turbidites beds: the influence of longitudinal flow structure. *Journal of Sedimentary Research*, **73**, 706–713.

Komar P.D. (1969) The channelized flow of turbidity currents with application to Monterey Deep-Sea Fan Channel. *Journal of Geophysical Research*, **74**, 4453–4599.

Komar P.D. (1971) Hydraulic jumps in turbidity currents. *GSA bulletin*, **82**, 1477–1488.

Lee S.E., Talling P.J., Ernst G.G.J. and Hogg A.J. (2002) Occurrence and origin of submarine plunge pools at the base of the US continental slope. *Marine Geology*, **185**, 363–377.

Leeuw J. de, Eggenhuisen J.T. and Cartigny M.J.B., (2016) Morphodynamics of Submarine Channel Inception Revealed by New Experimental Approach. *Nature Communications*, **7**, 10886.

Leeuw J. de, Eggenhuisen J. T. and Cartigny M. J. B. (2018) Linking submarine channel-levée facies and architecture to flow structure of turbidity current; insights from flume tank experiments. *Sedimentology*, **65**, 931–951.

Lowe D.R. (1982) Sediment gravity flows: II. Depositional models with special reference to the deposits of high-density turbidity currents, *Journal of Sedimentary Petrology*, **52**, 279–297.

Maier K.L., Fildani A., Paull C.K., McHargue T.R., Graham S.A. and Caress D.W. (2013) Deep-Sea Channel Evolution and Stratigraphic Architecture from Inception to

Abandonment from High-Resolution Autonomous Underwater Vehicle Surveys Offshore Central California. *Sedimentology*, **60**, 935–960.

Métivier F., Lajeunesse E. and Cacas M.C. (2005) Submarine canyons in the bathtub. *Journal of Sedimentary Research*, **75**, 6–11.

Mohrig D. and Buttles J. (2007) Deep Turbidity Currents in Shallow Channels. *Geology*, **35**, 155–158.

Mutti E. and Normark W. R. (1987) Comparing examples of modern and ancient turbidite systems: Problems and concepts. In: (Leggett J.K. eds.) *Marine clastic sedimentology* Chapter 1, pp 1–38.

Naruse, H. (2005). Usage and advantages of an application program STube for settling tube grain-size analysis. *Journal of the Sedimentological Society of Japan*, **62**, 55–61.

Nichols G. (2009) Sedimentology and Stratigraphy, 2nd edition. John Wiley & Sons, 432pp.

Niño Y., Lopez F. and Garcia M. (2003) Threshold for particle entrainment into suspension. *Sedimentology*, **50**, 247–263.

Normark W.R. (1970) Channel piracy on Monterey deep-sea fan. *Deep-Sea Research*, **17**, 837–846.

Normark W.R. and Gutmacher C.E., (1985) Delgada Fan: Preliminary interpretation of channel development. *Geo-Marine Letters*, **3**, 79–83.

Normark W.R., Hess G.R., Stow D.A.V. and Bowen A.J. (1980) Sediment waves on the Monterey Fan levee: a preliminary physical interpretation. *Marine Geology*, **37**, 1–18.

Peakall J., Amos K.J., Keevil G.M., Bradbury P.W. and Gupta S. (2007) Flow processes and sedimentation in submarine channel bends. *Marine and Petroleum Geology*, **24**, 470–486.

Pirmez C. and Imran J. (2003) Reconstruction of turbidity currents in Amazon Channel. *Marine and Petroleum Geology*, **20**, 823–849.

Posamentier, H. and Kolla, V. (2003) Seismic Geomorphology and Stratigraphy of Depositional Elements in Deep-Water Settings. *Journal of sedimentary research*, 73, 367–388.

Reading H. and Richard M. (1994) Turbidite Systems in Deep-Water Basin Margins Classified by Grain Size and Feeder System. *AAPG Bulletin*, **78**, 792–822.

Rowland J.C., Hilley G.E. and Fildani A. (2010) A Test of Initiation of Submarine Leveed Channels by Deposition Alone. *Journal of Sedimentary Research*, **80**, 710–727.

Shanmugam G. (2016) Submarine fans: a critical retrospective (1950-2015). *Journal of paleoceanography*, **5**, 110–184.

Shields A. (1936) Anwendung der Aehnlichkeitsmechanik und der Turbulenzforschung auf die Geschiebebewegung. Preussischen Versuchsanstalt für Wasserbau, Berlin, 26 pp.

Skene K.I, Piper D.J.W. and Hill P.S. (2002) Quantitative analysis of variations in depositional sequence thickness from submarine channel levées. *Sedimentology*, **49**, 1411–1430.

Spinewine B., Sun T., Babonneau N. and Parker G. (2011) Self-similar long profiles of aggrading submarine leveed channels: Analytical solution and its application to the Amazon channel. *Journal of Geophysical Research*, **116**, F03004, doi:10.1029/2010JF001937.

Straub K.M. and Mohrig D. (2008) Quantifying the morphology and growth of levees in aggrading submarine channels. *Journal of Geophysical Research-Earth Surface*, **113**, F03012, doi:10.1029/2007JF000896.

Wormleaton P.R., Hey R.D., Sellin R.H.J, Bryant T., Loveless J. and Catmur S.E. (2005) Behaviour of meandering overbank channels with graded sand beds. *Journal of Hydraulic Engineering*, **131**, 665–681.

Xu J.P. (2010) Normalized velocity profiles of field-measured turbidity currents. *Geology*, **38**, 563–566.

Yu B., Cantelli A., Marr J., Primez C., O'Byrne C. and Parker G. (2006) Experiments on self-channelized subaqueous fans emplaced by turbidity currents and dilute mudflows. *Journal of Sedimentary Research,* **76**, 889–902.

FIGURE CAPTIONS

Fig. 1. Schematic diagram of the experimental tank and setup.

コメントの追加 **[S4]:** On the figure, please change 'Siphon' to 'Syphon'

Fig. 2. Distribution of the grain-size diameter used in Experimental Series A, B, C and D (a total of 12 runs). Samples were taken from the mixing tanks.

Fig. 3. Locations of syphon sampling systems for measuring sediment concentration and flow velocity.

Fig. 4. Visual representation of the flow for (A) the first run without confinement and (B) the last run with confinement.

Fig. 5. Velocity and concentration profiles of the flow along the tank width. Measurements were recorded during the third run of the second experiment (B3).

Fig. 6. Photographs of the experimental tank after the experiment. (A) Topography formed in the tank after the end of the Experimental Series A. The area where bedforms are visible is the natural levée, and the channel and natural levée extend long downstream from the inlet. (B). Topography formed in the tank after the Experimental Series C. Bedforms are formed over the entire region, and channel-like landforms are formed only in a limited area near the inlet.

Fig. 7. Topography measured for the four experiments A, B, C and D. Dashed lines at 75 cm length represent the locations of the topographic sections shown in Figs 8 and 12.

Fig. 8. Topographic elevation measured along the transect at 75 cm for the four experimental series.

Fig. 9. Grain-size distribution along the channel and levée morphologies for all experiments. Coloured trend curves were associated with the same colour series data.

Fig. 10. Bedforms created after three consecutive runs of Series B.

Fig. 11. Schematic representation of the parameters *W* (width of the channel, distance between levée crests), *L* (length of the channel, distance from inlet to downstream axial deposit), and *H* (depth of the channel, distance between bottom of the channel and levée crest).

Fig. 12. Comparison between the morphologies of the levéed channels formed during the flume experiments and natural systems (Amazon channel, Jegou *et al.*, 2008; Villafranca channel, Hansel *et al.*, 2015; and Delgada channel, Normark & Gutmacher. 1983). Coordinates transverse to the channel elongation (*X*) and vertical coordinates (*Z*) are normalized by the width *W* of each channel.

Fig. 13. Shields diagram (Shields parameter as a function of the dimensionless Reynolds number) adapted from Leeuw *et al.* (2016).

Fig. 14. Schematic diagram indicating the influence of flow geometry on levée deposition. Arrows indicate the velocity vectors and the red lines are the contour lines for the velocity field. (A) line source inlet. The flow decelerates primarily at both ends of the expanding flow area, depositing natural levées. (B) Point source inlet. Because of the overall expansion of the flow, the depositional area of the natural levée becomes circular.

Appendix Figure A1. Velocity profiles taken at different locations along the centre of the channel (see Fig. 3 for locations) during the Series B, C and D.

Fig. 1.

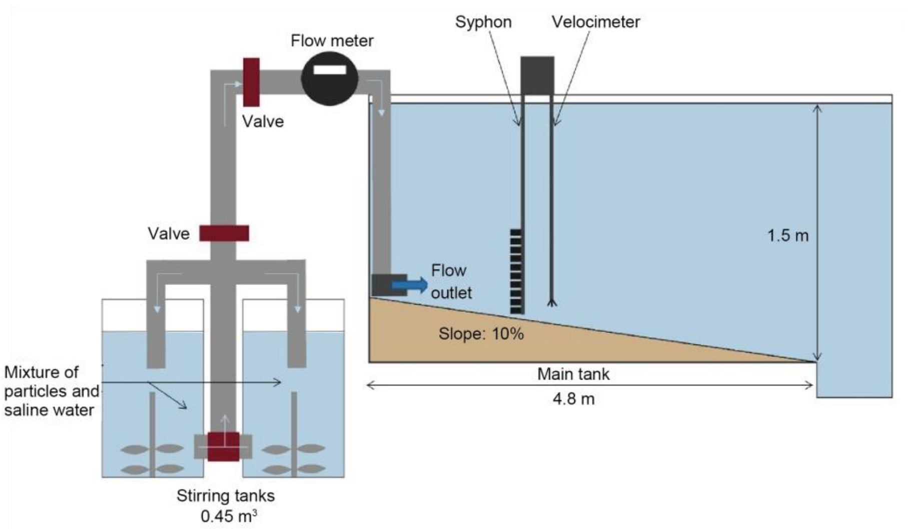

Syphon
Velocimeter
Flow meter
Valve
Valve
Flow
outlet
1.5 m
Slope: 10%
Mixture of
particles and
saline water
Main tank
4.8 m
Stirring tanks
0.45 m3

Fig. 2.

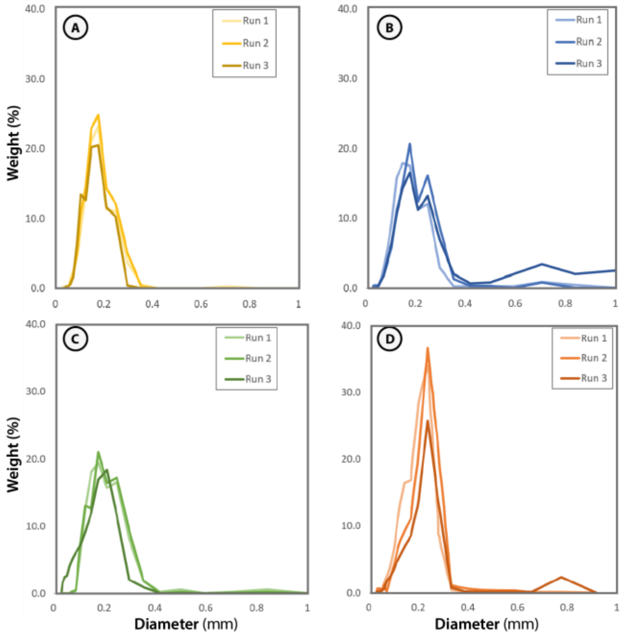

A
B
C
D
Run 1
Run 2
Run 3
Weight (%)
Diameter (mm)
0.0
10.0
20.0
30.0
40.0
0
0.2
0.4
0.6
0.8
1

Fig. 3

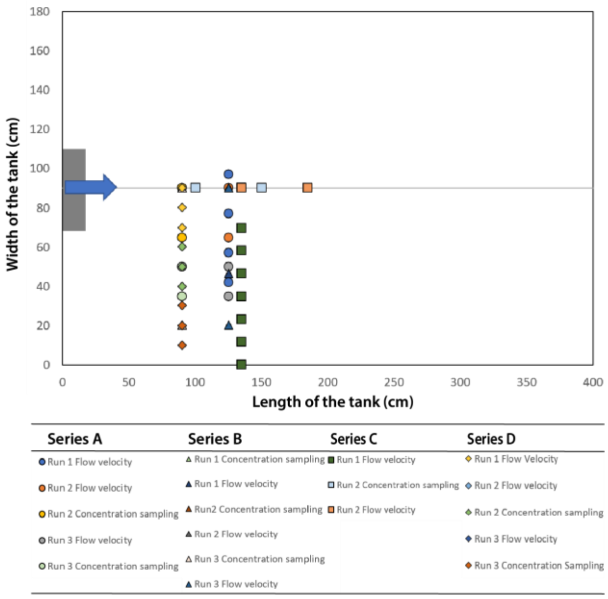

Width of the tank (cm)
Length of the tank (cm)
0
20
40
60
80
100
120
140
160
180
0
50
100
150
200
250
300
350
400
Series A
Run 1 Flow velocity
Run 2 Flow velocity
Run 2 Concentration sampling
Run 3 Flow velocity
Run 3 Concentration sampling
Series B
Run 1 Concentration sampling
Run 1 Flow velocity
Run2 Concentration sampling
Run 2 Flow velocity
Run 3 Concentration sampling
Run 3 Flow velocity
Series C
Run 1 Flow velocity
Run 2 Concentration sampling
Run 2 Flow velocity
Series D
Run 1 Flow Velocity
Run 2 Flow velocity
Run 2 Concentration sampling
Run 3 Flow velocity
Run 3 Concentration Sampling

Fig. 4.

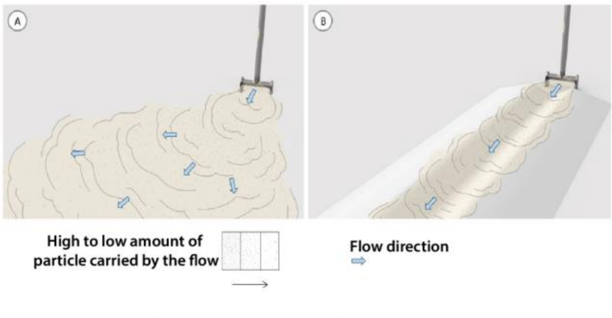
A
B
High to low amount of
particle carried by the flow
Flow direction

Fig. 5.

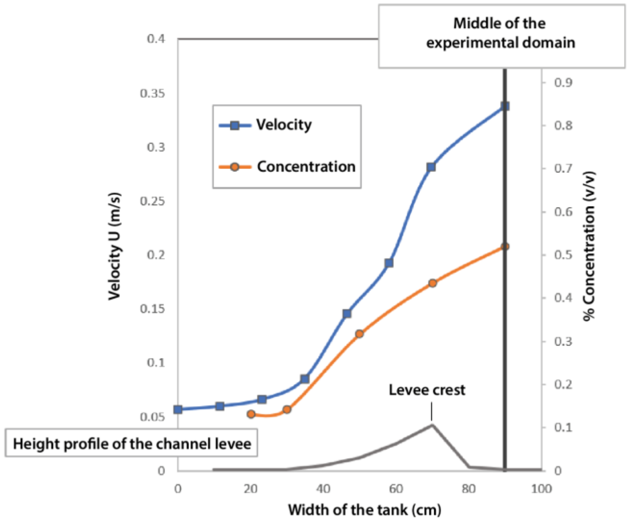
Middle of the experimental domain
Velocity
Concentration
Velocity U (m/s)
% Concentration (v/v)
Levee crest
Height profile of the channel levee
Width of the tank (cm)
0.4
0.35
0.3
0.25
0.2
0.15
0.1
0.05
0
0.9
0.8
0.7
0.6
0.5
0.4
0.3
0.2
0.1
0
0
20
40
60
80
100

Fig. 6.

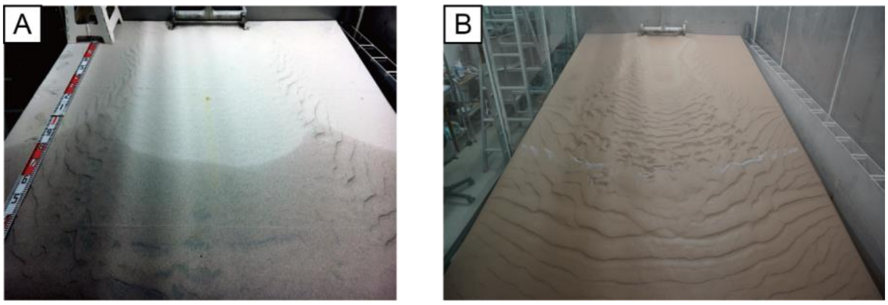

Fig. 7.

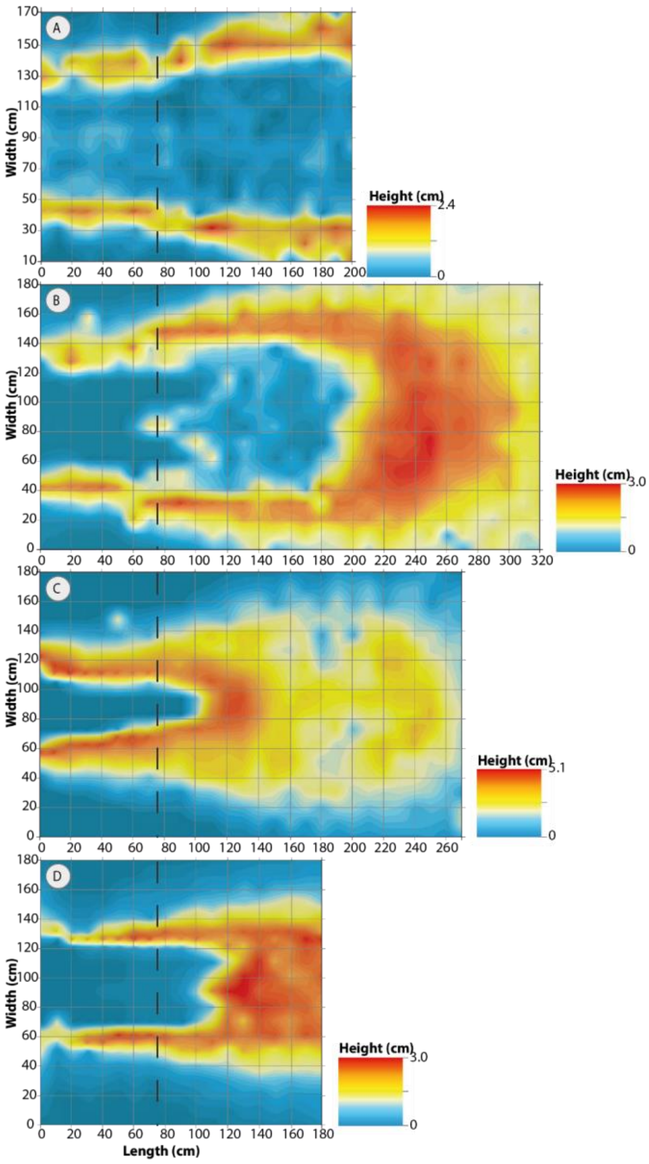

Fig. 8.

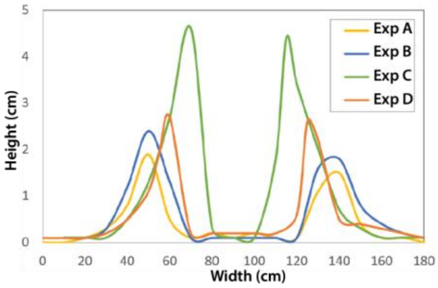
Exp A
Exp B
Exp C
Exp D
Height (cm)
Width (cm)
0
1
2
3
4
5
0
20
40
60
80
100
120
140
160
180

Fig. 9.

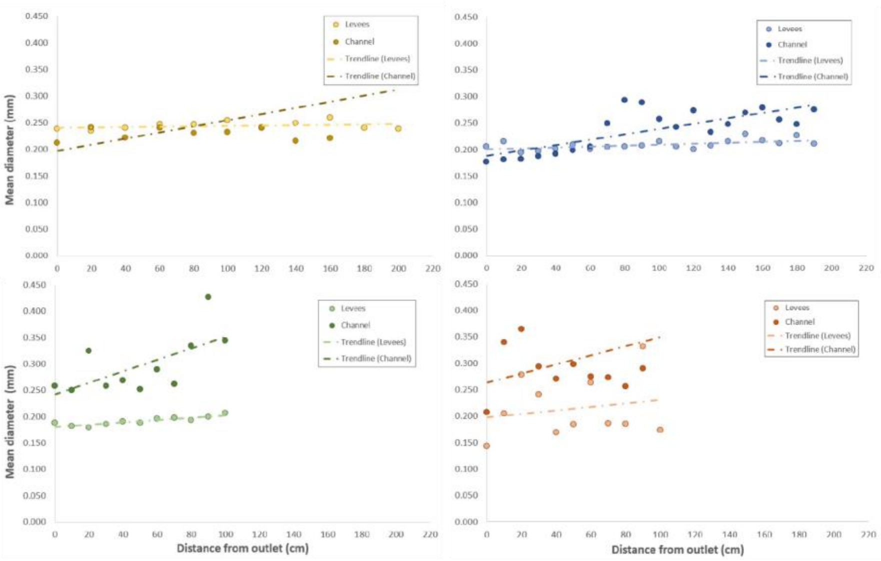

Levees
Channel
Trendline (Levees)
Trendline (Channel)
Mean diameter (mm)
Distance from outlet (cm)
0.000
0.050
0.100
0.150
0.200
0.250
0.300
0.350
0.400
0.450
0
20
40
60
80
100
120
140
160
180
200
220

Fig. 10.

Fig. 11.

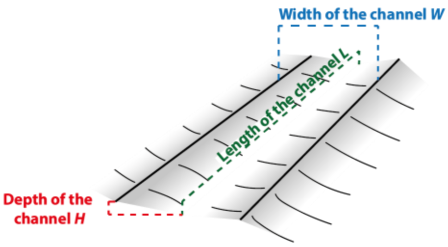
Width of the channel W
Length of the channel L
Depth of the channel H

Fig. 12.

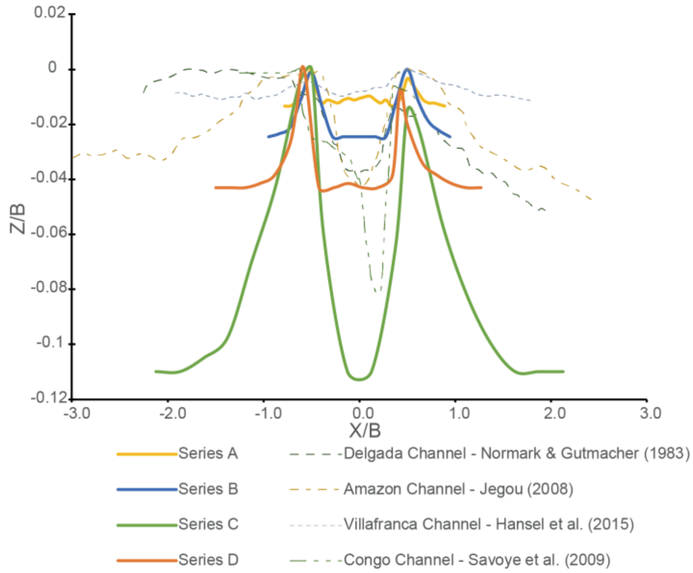

0.02
0
-0.02
-0.04
-0.06
-0.08
-0.1
-0.12
Z/B
-3.0
-2.0
-1.0
0.0
1.0
2.0
3.0
X/B
Series A
Series B
Series C
Series D
Delgada Channel - Normark & Gutmacher (1983)
Amazon Channel - Jegou (2008)
Villafranca Channel - Hansel et al. (2015)
Congo Channel - Savoye et al. (2009)

Fig. 13.

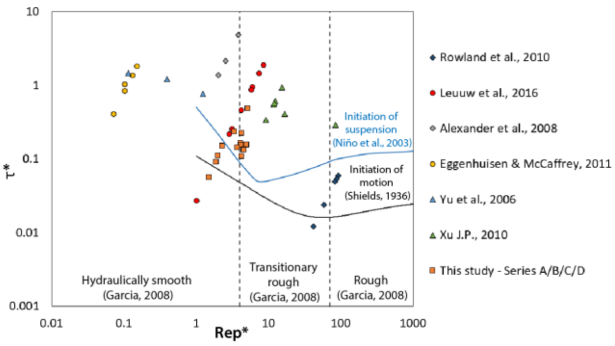

10
1
0.1
0.01
0.001
τ*
0.01
0.1
1
10
100
1000
Rep*
Hydraulically smooth
(Garcia, 2008)
Transitionary
rough
(Garcia, 2008)
Rough
(Garcia, 2008)
Initiation of
suspension
(Niño et al., 2003)
Initiation of
motion
(Shields, 1936)
Rowland et al., 2010
Leuuw et al., 2016
Alexander et al., 2008
Eggenhuisen & McCaffrey, 2011
Yu et al., 2006
Xu J.P., 2010
This study - Series A/B/C/D

Fig. 14.

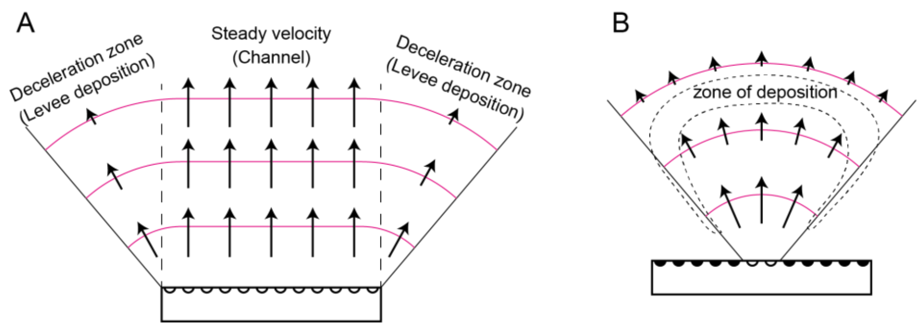
A
Deceleration zone
(Levee deposition)
Steady velocity
(Channel)
Deceleration zone
(Levee deposition)
B
zone of deposition

Fig. A1

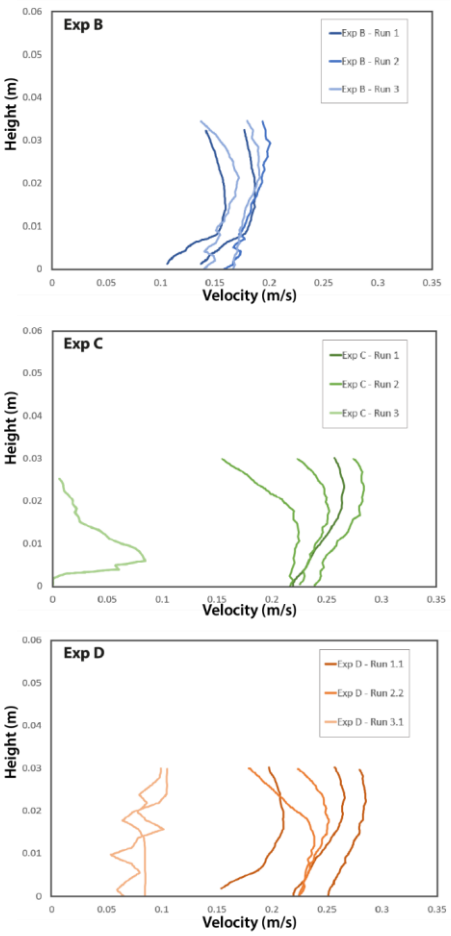
Exp B
Exp B - Run 1
Exp B - Run 2
Exp B - Run 3
Height (m)
Velocity (m/s)
Exp C
Exp C - Run 1
Exp C - Run 2
Exp C - Run 3
Height (m)
Velocity (m/s)
Exp D
Exp D - Run 1.1
Exp D - Run 2.2
Exp D - Run 3.1
Height (m)
Velocity (m/s)